Available online at www.sciencedirect.com
ScienceDirect
Trans. Nonferrous Met. Soc. China 32(2022) 1119−1132
Transactions of Nonferrous Metals Society of China
www.tnmsc.cn

Enhanced mechanical properties and formability of hot-rolled Mg−Zn−Mn alloy by Ca and Sm alloying

Wen-xue FAN[1], Yu BAI[1,2], Guang-yang LI[1], Xing-yang CHANG[1], Hai HAO[1,2]

1. School of Materials Science and Engineering, Dalian University of Technology, Dalian 116024, China;
2. Ningbo Research Institute of Dalian University of Technology, Ningbo 315016, China

Received 23 April 2021; accepted 7 December 2021

Abstract: In order to broaden the application of wrought Mg alloy sheets in the automotive industry, the influence of Ca and Sm alloying on the texture evolution, mechanical properties, and formability of a hot-rolled Mg−2Zn−0.2Mn alloy was investigated by OM, XRD, SEM, EBSD, tensile tests, and Erichsen test. The results showed that the average grain size and basal texture intensity of Mg−2Zn−0.2Mn alloys were remarkably decreased after Ca and Sm additions. 0.64 wt.% Ca or 0.48 wt.% Sm addition significantly increased the tensile strength, ductility and formability. Moreover, the synergetic addition of Sm and Ca improved the ductility and formability of Mg−2Zn−0.2Mn alloy, which was due to the change of Ca distribution and further reduction of the size of Ca-containing particles by Sm addition. The results provided a possibility of replacing RE elements with Ca and Sm in Mg alloys which bring about outstanding mechanical properties and formability.

Key words: Mg−Zn−Mn alloy; micro-alloying; hot rolling; texture evolution; formability

1 Introduction

In recent years, wrought magnesium alloys have received considerable attention in the automotive, electronics and aerospace industries, because of their excellent properties, including low density and high specific strength [1]. However, inherent hexagonal close-packed (HCP) structure [2,3] of magnesium alloys results in mediocre mechanical properties and poor formability at ambient temperature, which greatly restricts the practical applications of magnesium alloys. Therefore, how to improve the mechanical properties and formability of magnesium alloys is of great importance and has been a hot research topic so far. Grain refinement, second phase regulation and texture modification through alloying are beneficial to the formability of Mg alloys [4−6].

To date, many studies have been devoted to improving the stretch formability of Mg alloys by increasing the activity of non-basal slips and weakening texture [7−10]. In the recent studies, rare-earth (RE) elements have played an important role in grain refinement and texture weakening of Mg alloys and significantly improved the stretch formability of Mg alloys. The addition of 0.3 wt.% Sc to Mg−1.5Zn alloys significantly enhanced the stretch formability due to the weak basal textures [11]. Trace addition of Er in Mg−0.5Zn alloys can remarkably weaken the basal texture and 0.5 wt.% Er addition improved the stretch formability of Mg−0.5Zn alloy from 3.4 to 7.0 mm [12]. Experimental results also indicated that the addition of Y [13], Gd [14] and Ce [9] to Mg−Zn-based alloys could effectively weaken the strong basal texture and improve the stretch formability. Although many studies have shown that precious RE elements such as Gd, Y and Sc, can

Corresponding author: Yu BAI, Tel: +86-411-84709458, E-mail: ybai@dlut.edu.cn; Hai HAO, E-mail: haohai@dlut.edu.cn
DOI: 10.1016/S1003-6326(22)65860-6
1003-6326/© 2022 The Nonferrous Metals Society of China. Published by Elsevier Ltd & Science Press

significantly improve the strength and stretch formability of Mg−Zn alloys, the high price of RE elements would dramatically increase the costs of Mg alloys. Accordingly, more effort should be taken to find alternatives of RE elements to optimize the mechanical properties and formability of Mg alloys, thereby enhancing the future viability of Mg alloys.

Recently, due to the characteristic of Sm, such as small atomic radius difference between Mg, high solid solubility in magnesium alloy, and good solid solution strengthening effect, many works have been devoted to studying its effect on performance improvement of Mg alloys [15,16]. More importantly, inexpensive RE material with a low utilization coefficient has attracted more and more attention. $Mg_{41}Sm_5$ and $(Mg, Zn)_3Sm$ phases precipitated in Mg−Zn alloy after adding 1 wt.% Sm, which resulted in the grain refinement [17]. Besides, Sm has a significant effect on texture weakening. The texture intensity of Mg−Zn−Zr decreased significantly from 28.62 to 6.66 by adding 4 wt.% Sm [18]. Ca is another most commonly used alloying element in Mg alloys. It is reported that Ca addition in Mg−Zn alloys could not only refine the microstructure [19] and weaken the textures [20], but also improve the formability and mechanical properties [8]. The combined addition of RE and Ca elements is also reported to significantly modify the formability and enhance the strength [21−23]. Previous works have attempted to investigate the effect of micro-addition of Sm or Ca on the mechanical properties of Mg alloys [24,25]. The results showed that the Sm or Ca can significantly enhance the mechanical properties and weaken the basal texture of Mg alloys. It should also be noted that the prices of Sm and Ca are nearly a tenth of Gd and Y, so the addition of Sm and Ca alloying elements can replace expensive RE and could greatly reduce the cost of Mg alloy. However, investigations of the synergistic effect of Ca and Sm on microstructure modification, mechanical properties and formability in hot-rolled Mg alloys are rarely found so far.

The present study aims to comprehensively understand the influence of micro-alloying of Ca and Sm on mechanical properties of a hot-rolled Mg−2Zn−0.2Mn alloy and exploit a possibility of replacing the RE elements to low-priced elements in Mg alloys. On this basis, the contents of Ca and Sm were systematically changed and added to a Mg−2Zn−0.2Mn alloy, and the microstructure evolution, mechanical properties and formability were investigated in this study.

2 Experimental

Mg−2Zn−0.2Mn−X alloys (X: Ca and/or Sm) with different Ca and Sm contents were prepared by melting pure Mg, Zn (>99.96 wt.%), Mg−5Mn, Mg−30Sm, and Mg−20Ca master alloys (wt.%) under protection atmosphere of Ar at 730 °C inside an electric resistance furnace. The chemical compositions of the alloys were examined by an X-ray fluorescence analyzer (XRF−1800), as listed in Table 1. The 8 mm-thick plates for rolling were machined from the cast materials and subsequently homogenized at 400 °C for 12 h followed by water quenching. The unidirectional rolling process was carried out at 350 °C. The hot-rolled sheets were held at 350 °C for 10 min between every two rolling passes. The final thickness of the sheets was 1 mm with a total cumulative reduction of 87% over 11 passes. After rolling, a heat treatment at 350 °C for 1.5 h was conducted on all specimens to obtain a recrystallized structure. The schematic diagram of thermomechanical processes for fabricating 1 mm-thick Mg alloy sheets is shown in Figs. 1(a, b).

Specimens for microstructure observation were prepared by mechanical polishing and subsequent etching using a mixed solution of 5 mL acetic acid, 5 mL distilled water, 2.1 g picric acid,

Table 1 Chemical compositions of experimental alloys

Alloy number	Nominal composition/wt.%	Actual composition/wt.%				
		Zn	Mn	Ca	Sm	Mg
I	Mg−2Zn−0.2Mn	2.12	0.20	−	−	Bal.
II	Mg−2Zn−0.2Mn−0.5Ca	2.30	0.18	0.64	−	Bal.
III	Mg−2Zn−0.2Mn−1.0Ca	2.24	0.21	1.01	−	Bal.
IV	Mg−2Zn−0.2Mn−0.5Sm	2.26	0.24	−	0.48	Bal.
V	Mg−2Zn−0.2Mn−1.0Sm	2.03	0.22	−	0.98	Bal.
VI	Mg−2Zn−0.2Mn−0.5Ca−0.5Sm	1.97	0.26	0.56	0.61	Bal.

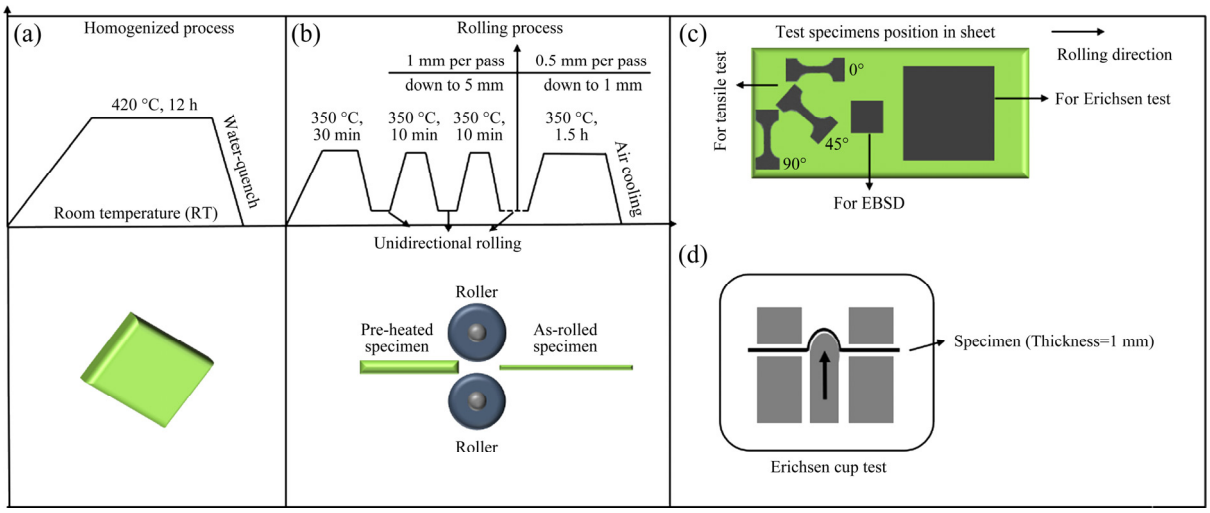

Fig. 1 Schematic diagram of thermomechanical process (a, b), position of specimens used for microstructure observation, tensile test and Erichsen test (c), and schematic illustration of Erichsen cup test (d)

and 35 mL ethanol. The phase identifications of samples were performed by X-ray diffraction (XRD, Empyrean 6000) using the Cu K_α radiation (λ=1.54 nm). Electron back scattering diffraction (EBSD) analysis was performed at an accelerating voltage of 20 kV, and step size of 1.5 μm. Before the EBSD analysis, all samples were mechanically polished by diamond paste and subsequently cleaned using an argon ion beam shower for 1.0 h under an applied voltage of 5 kV. The acquired EBSD data were analyzed with the software MTEX 4.5.2 [26]. The location of the specimens used for microstructure observation is shown in Fig. 1(c).

The tensile properties were investigated using a universal tensile test machine at an initial strain rate of 1×10^{-3} s^{-1} at ambient temperature. The tensile specimens' gauge length, width, and thickness were 12, 6, and 1 mm, respectively. The tensile specimens were machined from the annealed sheets along the rolling direction (RD), 45° to the RD, and 90° to the RD (along the transverse direction, TD), respectively, as shown in Fig. 1(c). To obtain reliable mechanical properties, the tensile test of each alloy was repeated three times.

Erichsen test (Fig. 1(d)) was performed to measure the formability at ambient temperature. The hemispherical punch was 20 mm in diameter. The stamping speed was set to 5 mm/min and the force of the holder was 10 kN. Graphite grease was used as the lubricant. The samples for the Erichsen tests were machined from the annealed sheets with 60 mm × 60 mm × 1 mm.

3 Results and discussion

3.1 Microstructure and texture

3.1.1 Microstructure

The XRD patterns of the hot-rolled alloy sheets are shown in Fig. 2. 0.5 wt.% Ca addition (Alloy II) resulted in the formation of the $Ca_2Mg_6Zn_3$ peaks in XRD results. Increasing Ca addition from 0.5 to 1 wt.% strengthened the $Ca_2Mg_6Zn_3$ peaks in the Alloy III. According to the previous research, Mg_2Ca precipitates tend to form when the molar ratio of Zn to Ca is below 1.2:1 in Mg−Zn−Ca systems [19]. In this study, even if 1.0 wt.% Ca was added to the Mg−2Zn−0.2Mn alloy, and the molar ratio of Zn to Ca was 2.2:1,

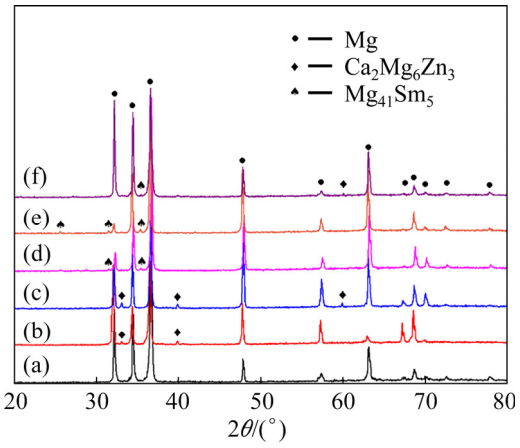

Fig. 2 XRD patterns of hot-rolled sheets with different Ca and Sm additions: (a) Alloy I; (b) Alloy II; (c) Alloy III; (d) Alloy IV; (e) Alloy V; (f) Alloy VI

which was still greater than 1.2:1. So, there were no Mg_2Ca phases formed in the Alloys II and III. Sm addition resulted in the weak $Mg_{41}Sm_5$ peaks in the Alloy IV. Even Sm content increased to 1 wt.%, there were no evident changes in the intensity of $Mg_{41}Sm_5$ peaks in the Alloy V. Also, it was interesting to note that the $Ca_2Mg_6Zn_3$ peaks cannot be obviously detected in the Alloy VI with Ca and Sm additions. Sm addition suppressed the $Ca_2Mg_6Zn_3$ formation. This may be the reason for the reduction of $Ca_2Mg_6Zn_3$ in the Alloy VI.

Figure 3 shows backscattered electron (BSE) images and EDS element distribution maps of the identical area in the corresponding BSE images of the as-rolled sheets of the Alloys II, IV and VI. Second phase particles with different chemical compositions having a diameter of several microns were observed in the above three samples. One was Zn- and Ca-enriched particles as indicated by white arrow-head 1 in Fig. 3(b), and the second one mainly contained Sm element as indicated by white arrow head 2 in Fig. 3(d). In Fig. 3(f), the particles indicated by white arrow heads 3 and 4 contained Zn, Ca and Sm elements. The particles in Fig. 3 were analyzed by EDS, and the results were summarized in Table 2. The Zn- and Ca-enriched particles in Alloy II were considered as $Ca_2Mg_6Zn_3$ phases. The RE-containing particles in the Alloy V may be $Mg_{41}Sm_5$ phases. These were consistent with the XRD results in Fig. 2. The results of EDS in Table 2 indicated that Sm addition into Mg−Zn−Mn−Ca alloy brought about the formation of a new second phase Mg−Zn−Ca−(Sm) containing Mg, Zn, Ca and Sm elements in Mg−2Zn−0.2Mn−0.5Ca−0.5Sm (Alloy VI), which was similar to the previous conclusion [27]. According to the EDS point analysis results in Table 2 and Figs. 3(e, f), the particles distributed along grain boundaries in Mg−2Zn−0.2Mn−0.5Ca−0.5Sm were the mixture of $Ca_2Mg_6Zn_3$ and Mg−Zn−Ca−(Sm) phases. Furthermore, the size of $Ca_2Mg_6Zn_3$ particles in Alloy VI was decreased by forming the new Mg−Zn−Ca−(Sm) phase consuming Ca atoms, resulting in a refinement effect of $Ca_2Mg_6Zn_3$ particles. For Alloy II, $Ca_2Mg_6Zn_3$ particles were distributed along grain boundaries and in α-Mg grains. It was remarkable that $Ca_2Mg_6Zn_3$ particles were favorably distributed along the α-Mg grain boundaries after Sm addition. The simultaneous presence of Sm and Ca can accelerate the formation of Mg−Zn−Ca−(Sm) particles, which consumed nearby Ca atoms and led to a change of Ca distribution. Furthermore, as the Sm element weakened the degree of recrystallization, the postponement of the recrystallization process can inhibit the precipitation of $Ca_2Mg_6Zn_3$ phases. As a result, the number of $Ca_2Mg_6Zn_3$ particles precipitated in Mg matrix was reduced.

Figure 4 shows the microstructure and the average grain size of the Mg−2Zn−0.2Mn−X (X: Ca and/or Sm) alloys rolled at 350 °C and subsequently annealed at 350 °C for 1.5 h. With 0.5 wt.% Ca addition, the grain size of Alloy II was reduced from 51.5 to 14.3 μm. With the further increase of Ca addition (1.0 wt.%), the grain size was refined to 9.0 μm. During the rolling process, the Ca-containing precipitates can restrain the dynamic recrystallization of Mg alloys, thereby playing the role of grain refinement [8,28]. Sm addition into the Mg−Zn alloys also played an important role in grain refinement, as reported in previous works[16,17]. Nevertheless, the grain refinement effect of Sm addition was not as strong as that of Ca addition. With the 1.0 wt.% Sm

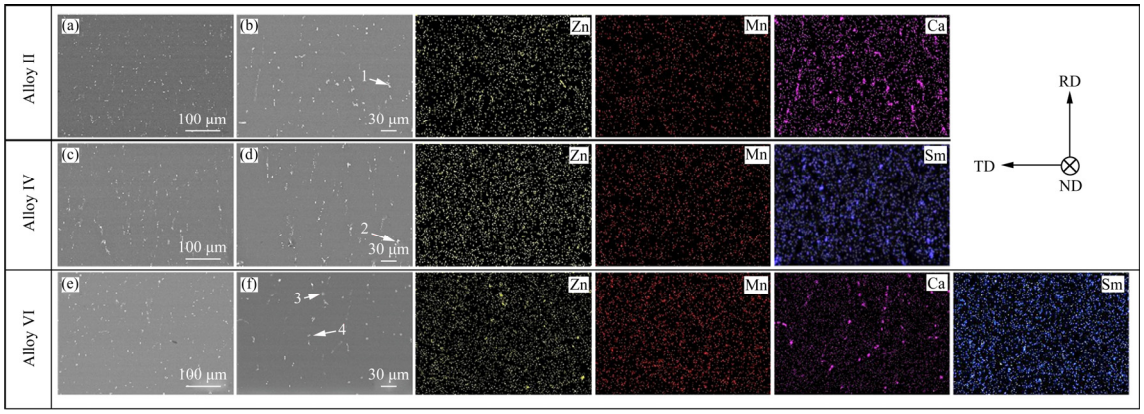

Fig. 3 BSE images and EDS element distribution maps of as-rolled sheets

Table 2 Chemical compositions of second phase particles indicated by white arrow heads in Fig. 3 (at.%)

Alloy No.	No.	Zn	Mn	Ca	Sm	Mg
II	1	17.38	0.07	12.33	−	Bal.
IV	2	3.89	0.04	−	9.69	Bal.
VI	3	16.23	0.10	11.08	1.26	Bal.
	4	18.44	0.03	9.21	2.01	Bal.

addition, the grain size of Alloy V was decreased to 15.0 μm. The grain size of Mg−2Zn−0.2Mn alloy can be reduced to 13.2 μm by the synergistic addition of 0.5 wt.% Ca and 0.5 wt.% Sm, which proved that Ca element had a stronger grain refining effect than Sm. There were equiaxed and fine grains in all samples after annealing. However, some twins were retained at room temperature, especially in Alloy I, Alloy IV, and Alloy V (Figs. 4(a, d and e)). For Mg−Zn alloys, $\{10\bar{1}2\}$ extension twins have the lowest critical resolved shear stress (CRSS) among all deformation modes, which can be easily activated when the degree of deformation increased. The activation of $\{10\bar{1}2\}$ extension twins can usually cause the 86.3° lattice rotation and generate a new twin-texture. In the present study, peaks were observed around 86.3° in the misorientation angle distribution maps, which testified to the existence of $\{10\bar{1}2\}$ extension twins. There were dislocation accumulations nearby twins due to the limited active slip systems under rolling deformation. The dislocation accumulations brought large strain energy storage, which can provide driving force for recrystallization. In general, recrystallization can give rise to weakening textures [29]. The previous study [30] has shown that trace rare earth elements can impede recrystallization during the rolling and annealing process, which resulted in residual twins in Alloy IV and Alloy V.

3.1.2 Texture evolution

EBSD measurements were conducted for the annealed samples to investigate texture evolution. The inverse pole figure (IPF) maps and corresponding (0001) pole figures of the annealed samples are shown in Fig. 5. The alloys with Ca and Sm additions exhibited finer microstructures, which was consistent with the microscopic observation (Fig. 4). For the different annealed alloys, there were noticeable different color distributions. Alloy I showed the most red-colored grains (Fig. 5(a)). By contrast, the Mg−2Zn−0.2Mn−Ca/Sm alloys contained grains with different colors, indicating a more randomly distributed orientation of grains. Due to the inherent HCP structure of Mg alloys with crystalline anisotropy, deformation is usually dominated by basal slip [31,32]. The (0001) pole figures demonstrated that the texture intensity of the annealed Mg−2Zn−0.2Mn alloys was reduced by adding Ca and Sm. 1 wt.% Ca addition decreased the (0001) texture intensity from 7.2 to 4.4. When Ca elements were added into alloys, the texture

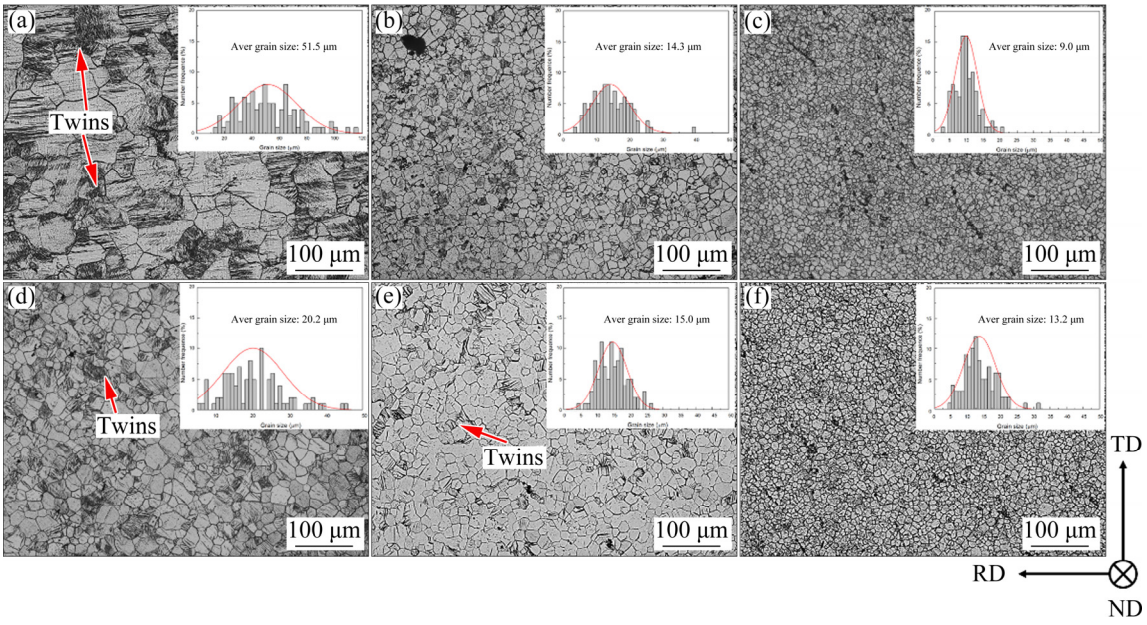

Fig. 4 Optical micrographs and average grain size of annealed sheets with different Ca and Sm additions: (a) Alloy I; (b) Alloy II; (c) Alloy III; (d) Alloy IV; (e) Alloy V; (f) Alloy VI

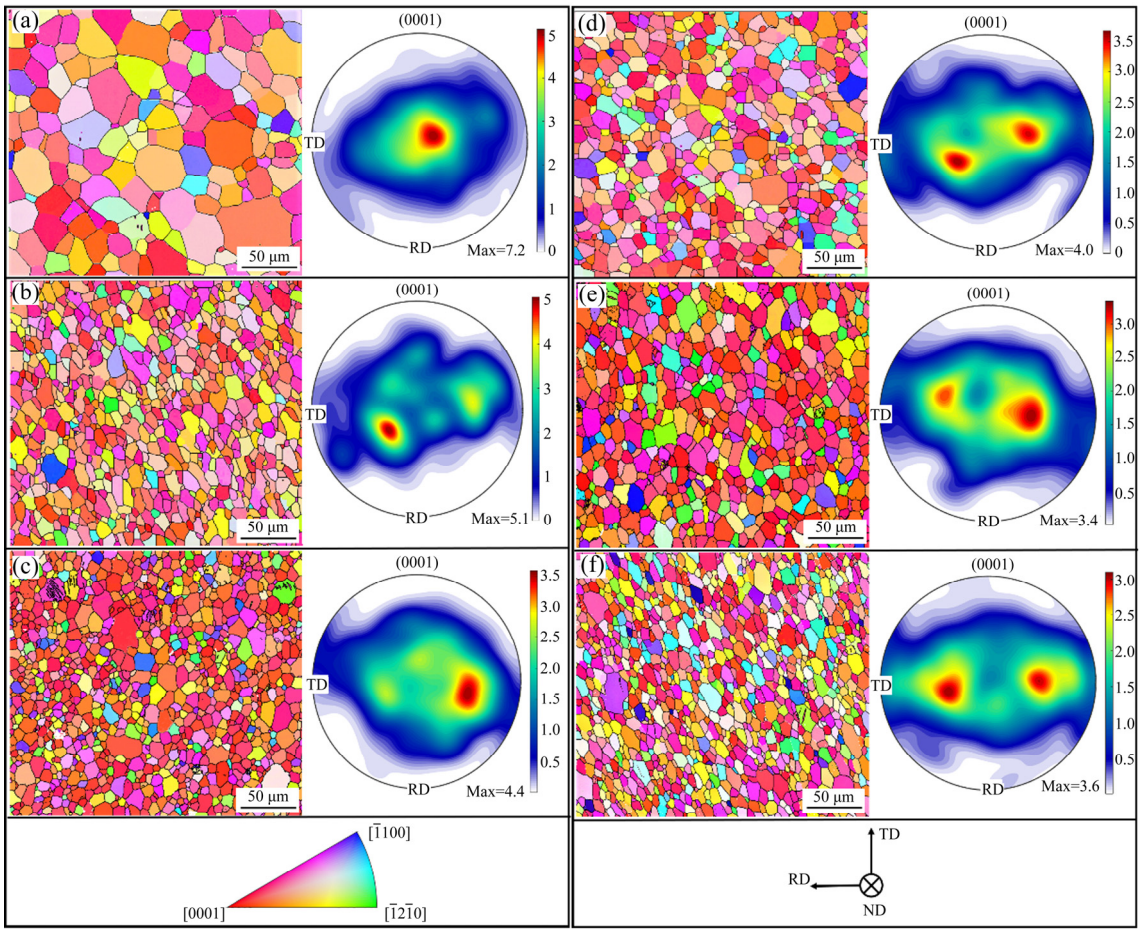

Fig. 5 Inverse pole figure (IPF) maps and (0001) pole figures of annealed sheets: (a) Alloy I; (b) Alloy II; (c) Alloy III; (d) Alloy IV; (e) Alloy V; (f) Alloy VI

intensities of Alloy II and Alloy III were reduced because of the slow diffusion rate and large atomic radius of Ca. The addition of Ca can significantly induce the local lattice distortion and the consequent decrease of the stacking fault energy (SFE), which benefitted from texture weakening [33]. It has been reported that texture weakening was probably induced by activating non-basal slips and twin-related recrystallization [34,35]. As shown in Figs. 5(d, e), the addition of 0.5 wt.% Sm and 1.0 wt.% Sm could weaken the texture intensity of the annealed Mg−2Zn−0.2Mn alloys to 4.0 and 3.4, respectively. The addition of RE elements could weaken the strong basal textures of wrought Mg alloys [36]. The Sm element enhanced the symmetry of HCP structure, thus promoting the activation of non-basal slips resulting in texture weakening. Also, most of the Mg−2Zn−0.2Mn−Ca/Sm alloy sheets exhibited the typical TD-split texture with double-peak intensity by about ±30° tilt. A strong basal texture is usually produced in magnesium alloys after rolling. As the degree of deformation increases, such a strong texture can selectively activate the $\langle c+a \rangle$ pyramidal slip and prismatic slip. When rolled Mg alloy sheet is subjected to repeated compression along with the TD during the rolling process, the development of TD spread of basal planes can be correlated with higher activity of prismatic slips [7]. In addition, AGNEW et al [37] also found that the activation of prismatic slips could also maintain the grains whose *c*-axis was parallel to the TD. Therefore, the increased TD tilted texture component is related to the activity of prismatic slips. Many studies have shown that the generation of TD-split texture is closely related to the deformation of grains and influenced by the subsequent annealing process [38,39]. During the rolling and subsequent annealing process, the grains having basal orientation disappeared based on the grain

nucleation and growth mechanism of recrystallization. Therefore, the grains with the TD tilted texture component remained. BOHLEN et al [40] also revealed that the formation of TD split texture is owing to the disappearance of the RD-split texture grains and remains TD-split texture grains during annealing.

Previous studies have shown that the recrystallization of Mg alloys resulted in the orientation rotation of 30° around the *c*-axis [41,42]. Grains grew up preferentially for nuclei rotated by ~30° around the *c* axis from $\langle 11\bar{2}0\rangle$ to $\langle 10\bar{1}0\rangle$ during the annealing process of Mg alloys [43]. Figure 6 shows the grain boundaries and misorientation angle distribution of the annealed alloys. The Mg−2Zn−0.2Mn−Ca/Sm alloys showed peaks at the misorientation angles of ~30° due to the six symmetries of magnesium alloy, which was consistent with the previous research [44], as shown in Figs. 6(b−d). It is known that the higher fraction of high-angle grain boundary (HAGB) in the wrought Mg alloy suggests the increased orientations among the grains. The lower fraction of low-angle grain boundaries (LAGB) means the stronger basal texture [45]. It can be seen from Fig. 6 that the misorientation angle distribution of alloys is mainly concentrated in two peaks (for example, (0°−5°) and (86±2)°). Mg−2Zn−0.2Mn alloy (Alloy I) with strong basal texture had a lower average misorientation angle compared to Alloys III, V and VI, as shown in Fig. 6. The average misorientation angle of Mg−2Zn−0.2Mn alloy increased from 28.67° to 36.48° and 42.13° with 1 wt.% Ca and 1 wt.% Sm additions, respectively. The average misorientation angle of Alloy VI also increased to 42.21° after the synergistic Ca and Sm addition. The higher content of HAGB in Alloys III, V and VI suggested the increased random orientations among the grains, indicating a weakening of texture. Therefore, it can be concluded that Ca and Sm addition can effectively weaken the basal texture of Mg−2Zn−0.2Mn alloy.

3.2 Mechanical property

3.2.1 Tensile properties

Engineering stress−strain curves for the Mg alloys obtained from the tensile tests are shown in Fig. 7. Planar anisotropy in strength and elongation can be found in all the alloys, especially in the yield strength (YS). The directional dependence of flow stress was likely to be primarily related to the texture [8]. The yield strengths along the RD direction of all investigated alloys were larger than those of the 45° and along the TD direction. 0.5 wt.% Ca addition increased the yield strength in all directions for Alloy II (Fig. 7(b)). According to the Hall−Petch relationship for Mg alloys, the decrease in grain size improves yield strength [46]. Increasing the addition of Ca to 1 wt.%, the yield strength further increased while the elongation decreased (Fig. 7(c)). The brittle Ca-containing particles can act as the source of crack initiation sites during the tensile deformation, resulting in decreased elongation [47]. Moreover, Ca addition could play a role in delaying and even hindering the dynamic recrystallization (DRX) process, which is harmful to the ductility [48]. For the Sm addition, both the YS and elongation increased with increasing the Sm content. Even though 1 wt.% Sm was added into the Alloy I, the yield strength was

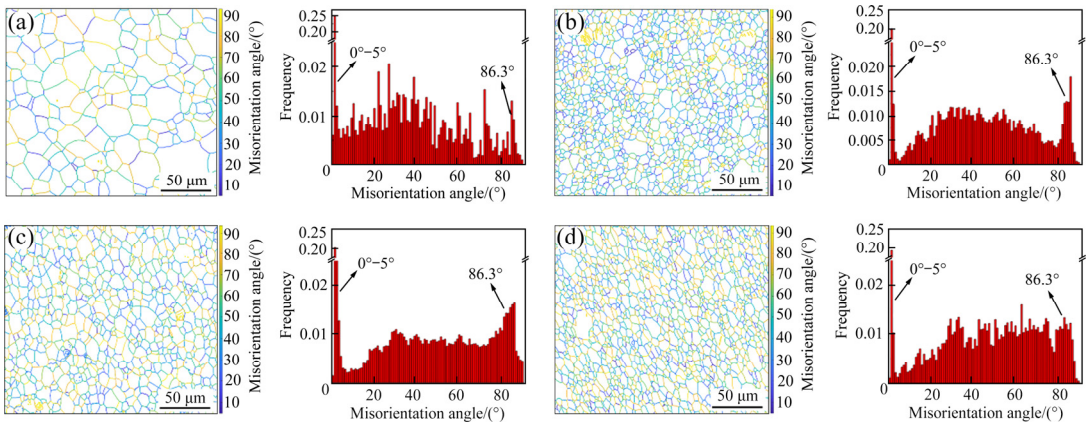

Fig. 6 Grain boundary information and misorientation angle distribution of annealed specimens: (a) Alloy I; (b) Alloy III; (c) Alloy V; (d) Alloy VI

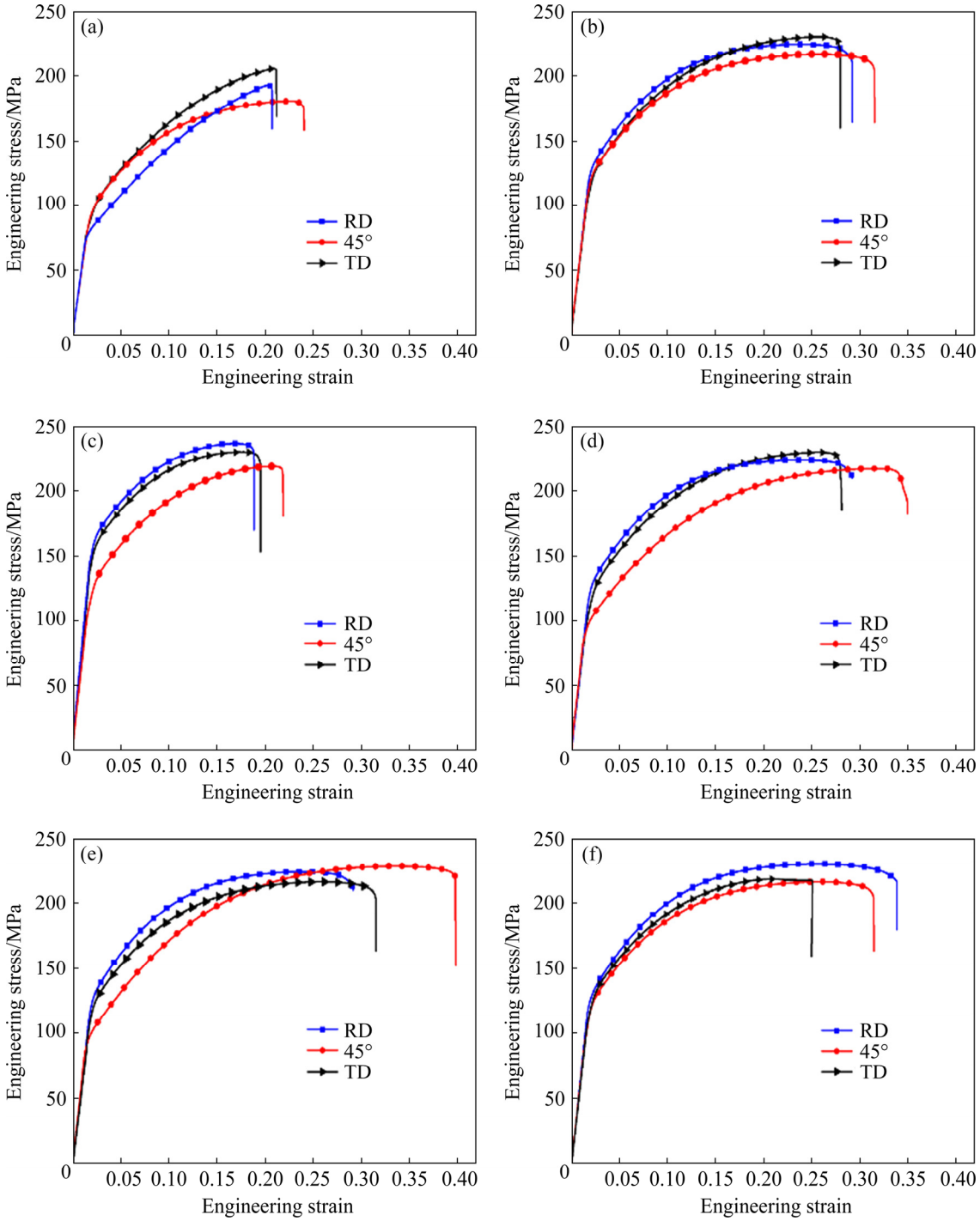

Fig. 7 Engineering stress−strain curves obtained by tensile tests of annealed samples at room temperature: (a) Alloy I; (b) Alloy II; (c) Alloy III; (d) Alloy IV; (e) Alloy V; (f) Alloy VI

still lower than that of the Alloy II, but the elongation was much higher than that of Alloy II. It can be concluded that the weakening of texture caused by addition of Sm was the main reason for the increase in elongation and the decrease in strength. For Alloy VI, the synergistic Sm and Ca addition improved the elongation of the alloy and maintained high strength.

The tensile properties for the investigated Mg alloys are summarized in Table 3, where the average strain-hardening exponent, n_{ave}, is given by $n_{ave}(=(n_{RD}+2n_{45°}+n_{TD})/4)$, where n_{RD}, $n_{45°}$ and n_{TD} are the strain hardening exponents at RD, 45° and TD), and the average Lankford value, r_{ave}, is given by $r_{ave}(=(r_{RD}+2r_{45°}+r_{TD})/4)$, where r_{RD}, $r_{45°}$ and r_{TD} are the Lankford values at RD, 45° and TD). The

Table 3 Tensile properties of annealed samples at room temperature (UTS: ultimate tensile stress; FE: elongation to failure; *n*: strain-hardening exponent; *r*: Lankford value)

Alloy	Direction	UTS/MPa	YS/MPa	FE/%	*n*	n_{ave}	*r*	r_{ave}
I	RD	194.45	76.10	20.75	0.24	0.28	1.24	1.81
	45°	181.76	87.97	24.02	0.31		2.01	
	TD	206.75	90.2	21.16	0.26		1.98	
II	RD	225.22	127.28	29.2	0.30	0.31	0.98	1.29
	45°	217.42	115.84	31.41	0.33		1.26	
	TD	231.40	112.96	27.97	0.29		1.65	
III	RD	236.66	154.73	19.96	0.29	0.29	1.42	1.59
	45°	219.46	117.42	21.93	0.33		1.33	
	TD	230.34	161.89	20.62	0.26		1.81	
IV	RD	224.8	127.7	29.26	0.37	0.34	0.96	1.02
	45°	218.69	94.07	35.09	0.34		1.02	
	TD	230.34	108.26	28.18	0.32		1.13	
V	RD	225.01	127.07	30.02	0.27	0.35	0.92	0.89
	45°	229.71	94.5	40.1	0.44		0.84	
	TD	217.42	123.21	31.55	0.36		0.89	
VI	RD	230.76	130.37	33.92	0.36	0.33	1.03	1.22
	45°	216.03	116.61	31.80	0.33		1.30	
	TD	219.04	121.17	25.60	0.29		1.24	

Lankford value and the strain hardening exponent are important indicators for evaluating formability. The *r* value of Alloy I was higher than other alloys, so it was difficult to reduce the thickness during the tensile test. The *n* values increased with the additions of Ca and Sm, which led to increased uniform plastic deformation. Moreover, except for Alloy I, the *n* values of all alloys increased in the order of $n_{RD}<n_{45°}<n_{TD}$ because of the different texture distribution. This was because the *c*-axis tilted texture promoted the formation of $\{10\bar{1}2\}$ tension twins and depressed the dynamic recovery [49].

Figure 8 shows the fracture morphologies of the tensile specimens. The cleavage planes were primarily observed in the Alloy I and Alloy III. Besides, it could be seen that many micro-cracks were found in these alloys, as shown in Figs. 8(a, c), especially in Alloy I. Finer grain sizes of the Alloy II and Alloy III resulted in higher yield strength. In contrast, the Alloy III exhibited lower elongation. The poor elongation of the Alloy III was related to the brittle Ca-containing particles [50]. Figure 9 shows the EDS results of points *A*, *B* and *C* in Figs. 8(b_1), (c_1) and (f_1). Due to the presence of the Ca element, Ca-containing particles would form in Alloy II, Alloy III and Alloy VI. As the content of Ca increased, the size of the particle phase would increase. The large Ca-containing particles served as the crack initiation sites and resulted in an earlier fracture in Alloy III, which deteriorated the elongation (Fig. 8(c_1)). Sm addition could affect Ca element distribution and reduce the Ca-containing particle size, as shown in Fig. 3. It can also be observed that there were some small-sized second phases at the bottom of the dimples (Figs. 8(b_1, c_1, f_1)). Due to the small size of the second phase, the elongations of the Alloy II and Alloy VI were less affected. There were many dimples in Alloy IV and Alloy V, suggesting that the fracture mechanism is ductile. Additionally, the Alloy V showed superior ductility with more uniformly distributed dimples.

3.2.2 Formability

Figure 10 shows the macroscopic appearances of the hot-rolled specimens with different Ca and Sm additions. There were obvious cracks at both edges of the Alloy I, which indicated the poor deformation ability of Mg−2Zn−0.2Mn alloy. After

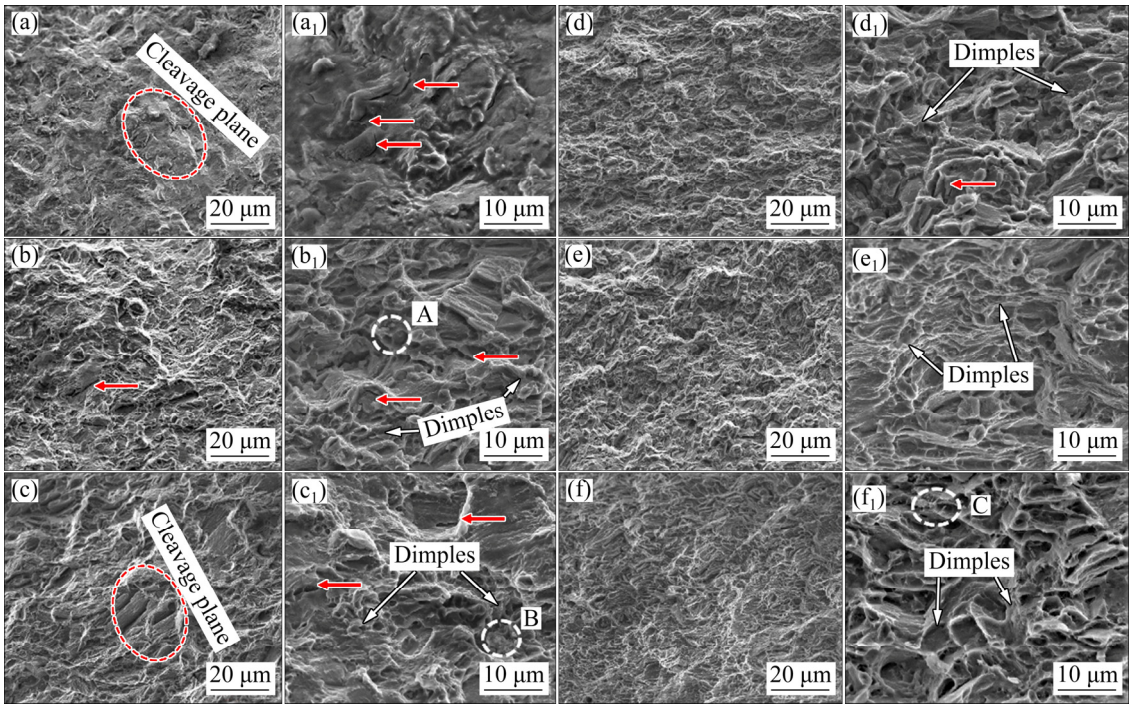

Fig. 8 Fracture morphologies of alloys along RD: (a) Alloy I; (b) Alloy II; (c) Alloy III; (d) Alloy IV; (e) Alloy V; (f) Alloy VI (The red arrows represent microcracks)

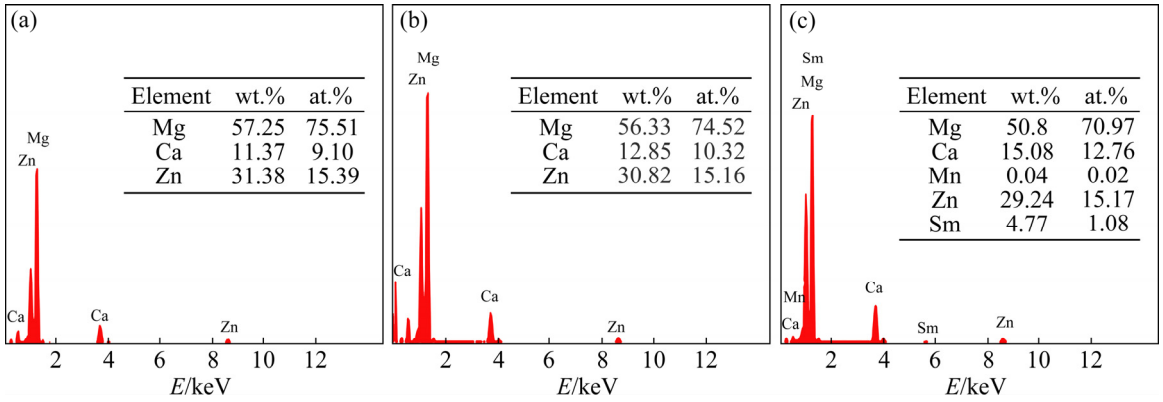

Fig. 9 EDS results of Points A (a), B (b), and C (c) in Figs. 8(b_1), (c_1) and (f_1)

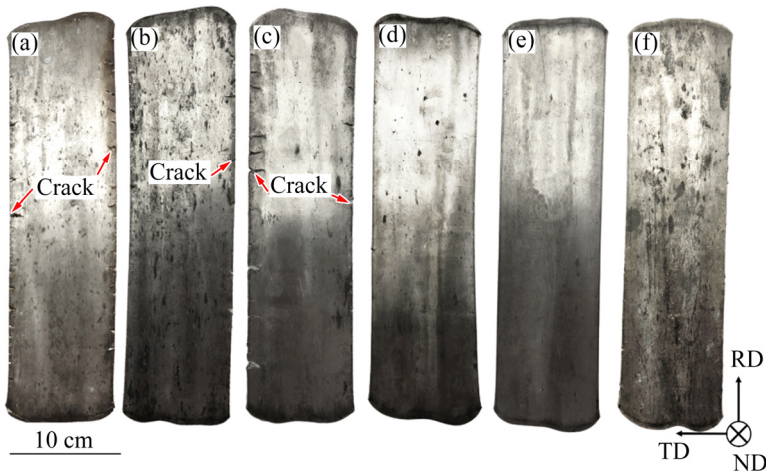

Fig. 10 Macroscopic appearance of hot-rolled sheets with different Ca and Sm additions: (a) Alloy I; (b) Alloy II; (c) Alloy III; (d) Alloy IV; (e) Alloy V; (f) Alloy VI

the addition of 0.5 wt.% Ca (Alloy II), the alloy exhibited improved deformation ability with a few edge cracks, which was attributed to the finer grain size in the Alloy II. Despite the finer grain size and weaker basal texture, cracking became serious by increasing the Ca content to 1.0 wt.% (Alloy III). This may be related to Ca-containing particles in alloys after adding Ca (Figs. 3(a, b)). In the case of the addition of Sm (Alloy IV and Alloy V), good appearances without cracks at the edge were achieved. For Alloy VI, there were fewer cracks compared to the Alloy II due to the more uniform Ca-containing particle distribution (Figs. 3(e, f)). Thus, it can be concluded that the Ca addition partly deteriorated the deformation ability of the Mg−2Zn−0.2Mn alloy, but the Sm addition improved the deformation ability.

Figure 11 shows the macro-photographs of the annealed specimens after the Erichsen tests. The addition of Ca and/or Sm significantly improved the formability of Mg−2Zn−0.2Mn alloy observed from the appearances. For Alloy I, the index Erichsen value (IE) at room temperature was 4.2 mm. The IE value significantly increased from 4.2 to 6.8 mm after 0.5 wt.% Ca addition. The previous study has shown that the weakened basal texture and the large splitting of the basal pole in the TD can improve the formability [50]. It is also suggested that grain refinement becomes the dominant factor for the excellent formability [51]. The 0.5 wt.% Ca addition effectively weakened the basal texture and reduced the grain size of Mg−2Zn−0.2Mn alloy, enhancing formability. However, the Ca addition to 1 wt.% (Alloy III) further increased, resulting in the decreased IE value of 5.5 mm, despite lower basal texture intensity and finer grain size. More Ca-containing particles formed in the Alloy III acted as the initiation of cracks during stretching, resulting in a decrease in formability. Benefitting from the significant basal texture weakening after 0.5 wt.% Sm addition, the basal texture of Mg−2Zn−0.2Mn alloy was significantly weakened from 5 to 3. The IE value was increased from 4.2 to 6.9 mm. With the further increase of the Sm content to 1 wt.% (Alloy V), the basal texture of alloy further weakened, and the IE value was 7.5 mm. In addition, the Alloy VI showed a high Erichsen value of 7.3 mm. Not only because it had a weak basal texture, but also the Sm addition affected the distribution of Ca-containing particles in the alloy. This significantly improved the sheet-thinning capability of Alloy VI.

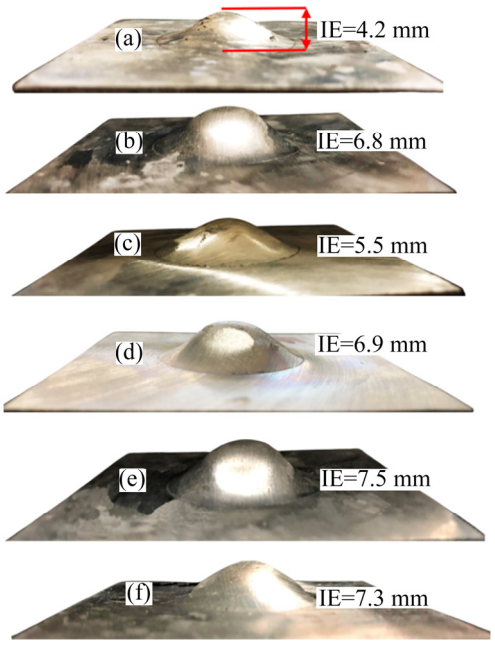

Fig. 11 Appearances and Erichsen values (IE) of annealed sheets after Erichsen tests: (a) Alloy I; (b) Alloy II; (c) Alloy III; (d) Alloy IV; (e) Alloy V; (f) Alloy VI

The larger r value indicates that it is more difficult to reduce the thickness of a sheet during the tensile process. The higher value of n means the lower sensitivity of strain localization, which indicates better elongation of the alloy [49,52]. There was no distinct difference in the r value between the Alloy II and Alloy III. Moreover, Alloy III exhibited a weak basal texture intensity. However, Alloy III showed a low Erichsen value of 5.5 mm. Therefore, the high content of Ca elements increased the number of Ca-containing particles in alloys, which can act as the crack initiation sites and result in the deterioration of the formability.

4 Conclusions

(1) $Ca_2Mg_6Zn_3$ and $Mg_{41}Sm_5$ phases formed in Mg−2Zn−0.2Mn alloy after the Ca and Sm additions. Increasing the additive amount of Ca and Sm from 0.5 to 1.0 wt.% caused an increase in the number of precipitates.

(2) The average grain sizes of Mg−2Zn−0.2Mn alloy remarkably decreased after Ca and Sm additions. Ca addition exerted a stronger effect on grain refinement than Sm addition.

(3) The basal texture of the annealed Mg−2Zn−0.2Mn alloy was significantly weakened with the Ca and Sm addition. Sm addition exhibited stronger texture weakening ability than Ca addition.

(4) Ca or Sm additions significantly improved the mechanical properties and formability of the Mg−2Zn−0.2Mn alloy. Further Ca addition deteriorated ductility and formability, while increasing Sm addition improved the formability. The synergistic addition of Sm and Ca improved the formability of Mg−2Zn−0.2Mn alloy.

Acknowledgments

This work was financially supported by the National Key Research and Development Program of China (Nos. 2018YFA0702903, 2016YFB0701-204), and the Fundamental Research Funds for the Central Universities, China (No. DUT20GF102).

References

[1] IMANDOUST A, BARRETT C D, AL-SAMMAN T, INAL K A, EL KADIRI H. A review on the effect of rare-earth elements on texture evolution during processing of magnesium alloys [J]. Journal of Materials Science, 2017, 52: 1−29.

[2] CHEN Yong-jun, WANG Qu-dong, LIN Jin-bao, LIU Man-ping, HJELEN J, ROVEN H J. Grain refinement of magnesium alloys processed by severe plastic deformation [J]. Transactions of Nonferrous Metals Society of China, 2014, 24: 3747−3754.

[3] WU Zhao-xuan, YIN Bing-lun, CURTIN W A. Energetics of dislocation transformations in hcp metals [J]. Acta Materialia, 2016. 119: 203−217.

[4] HAN Ting-zhuang, HUANG Guang-sheng, WANG You-gen, WANG Guan-gang, ZHAO Yan-chun, PAN Fu-sheng. Microstructure and formability evolutions of AZ31 magnesium alloy sheets undergoing continuous bending process [J]. Transactions of Nonferrous Metals Society of China, 2016, 26: 2043−2050.

[5] TAYLOR S, WEST G D, MOGIRE E, TANG F, KOTADIA H R. Superplastic forming characteristics of AZ41 magnesium alloy [J]. Transactions of Nonferrous Metals Society of China, 2021, 31: 648−654.

[6] LIU Bao-sheng, CAO Miao-miao, ZHANG Yue-zhong, HU Yong, GONG Chang-wei, HOU Li-feng, WEI Ying-hui. Microstructure, anticorrosion, biocompatibility and antibacterial activities of extruded Mg−Zn−Mn strengthened with Ca [J]. Transactions of Nonferrous Metals Society of China, 2021, 31: 358−370.

[7] SONG Bo, YANG Qing-shan, ZHOU Tao, CAI Lin-jiang, GUO Ning, LIU Ting-ting, GUO Sheng-feng, XIN Ren-long. Texture control by $\{10\bar{1}2\}$ twinning to improve the formability of Mg alloys: A review [J]. Journal of Materials Science & Technology, 2019, 35: 2269−2282.

[8] YUASA M, MIYAZAWA N, HAYASHI M, MABUCHI M, CHINO Y. Effects of group II elements on the cold stretch formability of Mg−Zn alloys [J]. Acta Materialia, 2015, 83: 294−303.

[9] LIU Peng, JIANG Hai-tao, CAI Zheng-xu, KANG Qiang, ZHANG Yun. The effect of Y, Ce and Gd on texture, recrystallization and mechanical property of Mg−Zn alloys [J]. Journal of Magnesium and Alloys, 2016, 4: 188−196.

[10] AL-SAMMAN T, LI X. Sheet texture modification in magnesium-based alloys by selective rare earth alloying [J]. Materials Science and Engineering A, 2011, 528: 3809−3822.

[11] BIAN Ming-zhe, HUANG Xin-sheng, MABUCHI M, CHINO Y. Compositional optimization of Mg−Zn−Sc sheet alloys for enhanced room temperature stretch formability [J]. Journal of Alloys and Compounds, 2020, 818: 152891.

[12] LIU Ke, LIANG Jing-tao, DU Wen-bo, LI Shu-bo, WANG Zhao-hui, YU Zi-jian, LIU Jin-xue. Microstructure, mechanical properties and stretch formability of as-rolled Mg alloys with Zn and Er additions [J]. Rare Metals, 2021, 40: 2179−2187.

[13] CHINO Y, SASSA K, MABUCHI M. Texture and stretch formability of a rolled Mg−Zn alloy containing dilute content of Y [J]. Materials Science and Engineering A, 2009, 513/514: 394−400.

[14] WU D, CHEN R S, HAN E H. Excellent room-temperature ductility and formability of rolled Mg−Gd−Zn alloy sheets [J]. Journal of Alloys and Compounds, 2011, 509: 2856−2863.

[15] GUAN Kai, MENG Fan-zi, QIN Peng-fei, YANG Q, ZHANG Dong-dong, LI Bai-shun, SUN W, LV Shu-hui, HUANG Yuan-ding, HORT N, MENG Jian. Effects of samarium content on microstructure and mechanical properties of Mg−0.5Zn−0.5Zr alloy [J]. Journal of Materials Science & Technology, 2019, 35: 1368−1377.

[16] XIA X Y, SANATY-ZADEH A, ZHANG C, LUO A A, ZENG X Q, CHANG Y A, STONE D S. Thermodynamic modeling and experimental investigation of the magnesium-zinc-samarium alloys [J]. Journal of Alloys and Compounds, 2014, 593: 71−78.

[17] ZHANG Tian-tian, CUI Hong-wei, CUI Xiao-li, CHEN Hong-mei, ZHAO Er-tuan, CHANG Li-li, PAN Yan-kun, FENG Rui, ZHAI Shen-bao, CHAI Shao-chun. Effect of addition of small amounts of samarium on microstructural evolution and mechanical properties enhancement of an as-extruded ZK60 magnesium alloy sheet [J]. Journal of Materials Research and Technology, 2020, 9: 133−141.

[18] ZHANG Tian-tian, CUI Hong-wei, CUI Xiao-li, CHEN Hong-mei, ZHAO Er-tuan, PAN Yan-kun, FENG Rui, JIA Qiu-rong, ZHAO J. Ductility enhancement in an as-extruded Mg−5.5Zn−0.8Zr alloy by Sm alloying [J]. Journal of Alloys and Compounds, 2019, 784: 1130−1138.

[19] DING Han-lin, ZHANG Peng, CHENG Guang-ping, KAMADO S. Effect of calcium addition on microstructure and texture modification of Mg rolled sheets [J]. Transactions of Nonferrous Metals Society of China, 2015, 25: 2875−2883.

[20] GUAN Di-kai, LIU Xiang-guang, GAO Jun-heng, MA Le, WYNNE B P, RAINFORTH W M. Exploring the

mechanism of “Rare Earth” texture evolution in a lean Mg−Zn−Ca alloy [J]. Scientific Reports, 2019, 9: 7152.

[21] NAKATA T, LI Z H, SASAKI T, HONO K, KAMADO S. Room-temperature stretch formability, tensile properties, and microstructures of precipitation hardenable Mg−6Zn−0.2Ca (mass%) alloy sheets micro-alloyed with Ce or Y [J]. Materials Science and Engineering A, 2021, 804: 140563.

[22] CHU J H, TONG L B, JIANG Z H, ZOU D N, WANG Q J, LIU S F, ZHANG H J. A comparison study of Ce/La and Ca microalloying on the bio-corrosion behaviors of extruded Mg−Zn alloys [J]. Journal of Magnesium and Alloys, 2020, 8: 1269−1280.

[23] NAKATA T, XU C, UEHARA Y, SASAKI T T, KAMADO S. Origin of texture weakening in a rolled ZEX4101 alloy sheet and its effect on room temperature formability and tensile property [J]. Journal of Alloys and Compounds, 2019, 782: 304−314.

[24] FU Li, LE Qi-chi, HU Wen-xin, ZHANG Jun, WANG Jian-ming. Strengths and ductility enhanced by micro-alloying Sm/La/Ca to Mg−0.5Zn−0.2Mn alloy [J]. Journal of Materials Research and Technology, 2020, 9(3): 6834−6849.

[25] LIU Xiao-huan, XU Rui. Achieving ultra-high hardness of Mg−Sm−Ca alloy with the unique nanostructure [J]. Materials Science and Engineering A, 2021, 825: 141929.

[26] BACHMANN F, HIELSCHER R, SCHAEBEN H. Texture analysis with MTEX-free and open source software toolbox [J]. Solid State Phenomena, 2010, 160: 63−68.

[27] TONG L B, ZHANG Q X, JIANG Z H, ZHANG J B, MENG J, CHENG L R, ZHANG H J. Microstructures, mechanical properties and corrosion resistances of extruded Mg−Zn−Ca−*x*Ce/La alloys [J]. Journal of the Mechanical Behavior of Biomedical Materials, 2016, 62: 57−70.

[28] DING Tian, YAN Hong-ge, CHEN Ji-hua, XIA Wei-jun, SU Bin, YU Zong-lin. Dynamic recrystallization and mechanical properties of high-strain-rate hot rolled Mg–5Zn alloys with addition of Ca and Sr [J]. Transactions of Nonferrous Metals Society of China, 2019, 29: 1631−1640.

[29] ZHU S Q, YAN H G, CHEN J H, WU Y Z, LIU J Z, TIAN J. Effect of twinning and dynamic recrystallization on the high strain rate rolling process [J]. Scripta Materialia, 2010, 63: 985−988.

[30] GAO Lei, YANG Hong, LUO Jun, LUO A A, CHEN Rong-shi. Microstructure and mechanical properties of a high ductility Mg−Zn−Mn−Ce magnesium alloy [J]. Journal of Magnesium and Alloys, 2013, 1: 283−291.

[31] GUAN Di-kai, RAINFORTH W M, MA Le, WYNNE B, GAN Jun-heng. Twin recrystallization mechanisms and exceptional contribution to texture evolution during annealing in a magnesium alloy [J]. Acta Materialia, 2017, 126: 132−144.

[32] ZENG Zhuo-ran, BIAN M Z, XU S W, DAVIES C H J, BIRBILIS N, NIE Jin-feng. Effects of dilute additions of Zn and Ca on ductility of magnesium alloy sheet [J]. Materials Science and Engineering A, 2016, 674: 459−471.

[33] DING Han-lin, SHI Xiao-bin, WANG Yong-qiang, CHENG Guang-ping, KAMADO S. Texture weakening and ductility variation of Mg−2Zn alloy with CA or RE addition [J]. Materials Science and Engineering A, 2015; 645: 196−204.

[34] HUANG Xin-sheng, SUZUKI K, CHINO Y. Influences of initial texture on microstructure and stretch formability of Mg−3Al−1Zn alloy sheet obtained by a combination of high temperature and subsequent warm rolling [J]. Scripta Materialia, 2010, 63: 395−398.

[35] HUANG Xin-sheng, SUZUKI K, CHINO Y. Static recrystallization behavior of hot-rolled Mg−Zn−Ce magnesium alloy sheet [J]. Journal of Alloys and Compounds, 2017, 724: 981−990.

[36] GRIFFITHS D. Explaining texture weakening and improved formability in magnesium rare earth alloys [J]. Materials Science and Technology, 2015, 31: 10−24.

[37] AGNEW S R, YOO M H, TOMÉ C N. Application of texture simulation to understanding mechanical behavior of Mg and solid solution alloys containing Li or Y [J]. Acta Materialia, 2001, 49: 4277−4289.

[38] MACKENZIE L W F, PEKGULERYUZ M O. The recrystallization and texture of magnesium-zinc-cerium alloys [J]. Scripta Materialia, 2008, 59: 665−668.

[39] CHINO Y, HUANG Xin-sheng, SUZUKI K, SASSA K, MABUCHI M. Influence of Zn concentration on stretch formability at room temperature of Mg−Zn−Ce alloy [J]. Materials Science and Engineering A, 2010, 528: 566−572.

[40] BOHLEN J, WENDT J, NIENABER M, KAINER K U, STUTZ L, LETZIG D. Calcium and zirconium as texture modifiers during rolling and annealing of magnesium-zinc alloys [J]. Materials Characterization, 2015, 101: 144−152.

[41] TONG L B, ZHENG M Y, CHENG L R, ZHANG D P, KAMADO S, MENG J, ZHANG H J. Influence of deformation rate on microstructure, texture and mechanical properties of indirect-extruded Mg−Zn−Ca alloy [J]. Materials Characterization, 2015, 104: 66−72.

[42] STEINER M A, BHATTACHARYYA J J, AGNEW S R. The origin and enhancement of $\{0001\}\langle 11\bar{2}0\rangle$ texture during heat treatment of rolled AZ31B magnesium alloys [J]. Acta Materialia, 2015, 95: 443−455.

[43] BISWAS S, BEAUSIR B, TOTH L S, SUWAS S. Evolution of texture and microstructure during hot torsion of a magnesium alloy [J]. Acta Materialia, 2013, 61: 5263−5277.

[44] WANG Guan-gang, HUANG Guang-sheng, CHEN Xiang, DENG Qian-yuan, TANG Ai-tao, JIANG Bin, PAN Fu-sheng. Effects of Zn addition on the mechanical properties and texture of extruded Mg−Zn−Ca−Ce magnesium alloy sheets [J]. Materials Science and Engineering A, 2017, 705: 46−54.

[45] ZHAO Hong-liang, HUA Yun-xiao, DONG Xiang-lei, XING Hui, LU Yan-li. Influence of trace Ca addition on texture and stretch formability of AM50 magnesium alloy sheet [J]. Transactions of Nonferrous Metals Society of China, 2020, 30: 647−656.

[46] HAO Hai, LIU Xiao-teng, FANG Can-feng, ZHANG Xing-guo. Effect of in-situ Al_2Y particles on the as-cast/as-rolled microstructure and mechanical properties of AZ31 alloy [J]. Materials Science and Engineering A, 2017, 698: 27−35.

[47] ZHOU Meng-ran, HUANG Xin-sheng, MORISADA Y, FUJII H, CHINO Y. Effects of Ca and Sr additions on microstructure, mechanical properties, and ignition temperature of hot-rolled Mg−Zn alloy [J]. Materials Science and Engineering A, 2020, 769: 138474.

[48] DU Y Z, QIAO X G, ZHENG M Y, WANG D B, WU K, GOLOVIN I S. Effect of microalloying with Ca on the microstructure and mechanical properties of Mg−6 mass% Zn alloys [J]. Materials & Design, 2016, 98: 285−293.
[49] WANG Guan-gang, HUANG Guang-sheng, HUANG Yu, ZHANG Cheng, JIANG Bin, TANG Ai-tao, PAN Fu-sheng. Achieving high ductility in hot-rolled Mg−*x*Zn−0.2Ca−0.2Ce sheet by Zn addition [J]. JOM, 2020, 72: 1607−1618.
[50] CHINO Y, UEDA T, OTOMATSU Y, SASSA K, HUANG X S, SUZUKI K, MABUCHI M. Effects of Ca on tensile properties and stretch formability at room temperature in Mg−Zn and Mg−Al alloys [J]. Materials Transactions, 2011, 52: 1477−1482.
[51] LI Zi-han, ZHOU Guo-wei, LI Da-yong, WANG Hua-miao, TANG Wei-qin, PENG Ying-hong, ZUROB H S, WU Pei-dong. Crystal plasticity based modeling of grain boundary sliding in magnesium alloy AZ31B sheet [J]. Transactions of Nonferrous Metals Society of China, 2021, 31: 138−155.
[52] HUANG Xin-sheng, SUZUKI K, CHINO Y, MABUCHI M. Improvement of stretch formability of Mg−3Al−1Zn alloy sheet by high temperature rolling at finishing pass [J]. Journal of Alloys and Compounds, 2011, 509: 7579−7584.

Ca 和 Sm 合金化增强 Mg−Zn−Mn 合金的力学性能和成形性能

范文学[1]，白 玉[1,2]，李广阳[1]，常星阳[1]，郝 海[1,2]

1. 大连理工大学 材料科学与工程学院，大连 116024；
2. 大连理工大学 宁波研究院，宁波 315016

摘 要：为了拓宽变形镁合金板材在汽车工业中的应用，通过光学显微镜(OM)、X 射线衍射仪(XRD)、扫描电子显微镜(SEM)、电子背散射衍射技术(EBSD)、拉伸试验和杯突试验，研究 Ca 和 Sm 合金化对热轧 Mg−2Zn−0.2Mn 合金的织构演变、力学性能和成形性的影响。结果表明，添加 Ca 和 Sm 后，Mg−2Zn−0.2Mn 合金的平均晶粒尺寸减小，基面织构强度显著降低。添加 0.64% Ca 或 0.48% Sm(质量分数)能显著提高 Mg−2Zn−0.2Mn 合金的拉伸强度、塑性和成形性。此外，Sm 和 Ca 的协同作用可以进一步改善 Mg−2Zn−0.2Mn 合金的塑性和成形性，这是由于 Sm 的添加可以影响 Ca 的分布并减少含 Ca 颗粒的尺寸。研究结果为在镁合金中利用 Ca 和 Sm 替代贵重稀土元素提供了可能性，进而带来优异的力学性能和成形性能。

关键词：Mg−Zn−Mn 合金；合金化；热轧；织构演变；成形性

(Edited by Xiang-qun LI)